Journal of Applied Physics ARTICLE scitation.org/journal/jap

Depth profiles of electron traps generated during reactive ion etching in n-type 4H-SiC characterized by using isothermal capacitance transient spectroscopy

Cite as: J. Appl. Phys. **130**, 105703 (2021); doi: 10.1063/5.0059588
Submitted: 10 June 2021 · Accepted: 17 August 2021 ·
Published Online: 9 September 2021

Kazutaka Kanegae,[1,a)] Takafumi Okuda,[1] Masahiro Horita,[2,3] Jun Suda,[1,2,3] and Tsunenobu Kimoto[1]

AFFILIATIONS

[1]Department of Electronic Science and Engineering, Kyoto University, Nishikyo, Kyoto 615-8510, Japan
[2]Institute of Materials and Systems for Sustainability (IMaSS), Nagoya 464-8601, Japan
[3]Department of Electronics, Nagoya University, Nagoya 464-8601, Japan

[a)]**Author to whom correspondence should be addressed:** kanegae@semicon.kuee.kyoto-u.ac.jp

ABSTRACT

Electron traps generated during the reactive ion etching (RIE) process in n-type 4H-SiC are investigated using the deep-level transient spectroscopy technique and isothermal capacitance transient spectroscopy (ICTS) technique. Two electron traps of the $Z_{1/2}$ center ($E_C - 0.64$ eV) and the EH_3 center ($E_C - 0.74$ eV) are detected in the RIE-etched sample by ICTS measurement at 300 K. A method is proposed to determine the depth profiles of the electron traps that are localized near the etched surface, whereby a depth profile is extracted from the dependence of averaged trap density on the depletion layer width. An exponential distribution is assumed as the depth profile of the electron traps generated during the RIE process. The extracted depth profile was confirmed to be consistent with that determined by the double-correlation method. An appropriate function for the depth profile of carrier traps is assumed and the dependence of the averaged trap density on the depletion layer width is analyzed, which enables the extraction of a depth profile that has both higher depth resolution and higher resolution in the carrier trap density with the proposed method than that with the double-correlation method.

I. INTRODUCTION

Silicon carbide (SiC) has attracted much attention for use in power devices because of its significant advantages, such as a high critical electric field and a wide range of doping control for n- and p-type conductivities.[1–5] SiC Schottky barrier diodes (SBDs) and metal-oxide-semiconductor field effect transistors (MOSFETs) have been commercialized by several manufacturers. Reactive ion etching (RIE) is an essential process for the fabrication of such SiC devices to form mesa and trench structures. However, lattice damage produced by ion bombardment is a concern for the development of SiC devices. For example, a reduction in barrier height and degradation in the forward characteristics due to RIE damage in 4H-SiC SBDs have been reported.[6] Carrier traps generated during the RIE process, unlike those created during ion implantation processes,[7–9] are localized near the etched surface (<1 μm) and may have steep depth profiles.

In deep-level transient spectroscopy (DLTS)[10] and isothermal capacitance transient spectroscopy (ICTS)[11] techniques, which are generally employed to characterize deep levels that act as carrier traps, it is typically assumed that the carrier trap density in a detection region is constant.[12,13] In contrast, the double-correlation method[14] has been employed[9,15–19] when a carrier trap density shows a spatial distribution in the depth direction. However, the double-correlation method has a trade-off relationship between the depth resolution and the resolution in the carrier trap density due to the measurement principle. Therefore, it is difficult to investigate a steep depth profile, such as in the case of carrier traps induced during RIE processes. Reports on detailed depth profiles of carrier traps generated during RIE processes in 4H-SiC have been limited.[19] In this study, we perform ICTS measurement with various measurement bias voltages for RIE-etched samples and

analyze the ICTS data assuming appropriate shapes of the depth profiles. The depth profiles of the electron traps generated during the RIE process in n-type 4H-SiC are thus extracted.

II. THEORETICAL AND EXPERIMENTAL APPROACH

When an n-type SBD is used to investigate electron traps with capacitance transient spectroscopy, the electron trap density in the detection region calculated from DLTS or ICTS peak intensity ($\tilde{N}_T$) has the following relationship with the depth profile of an actual trap density [$N_T(x)$], where x is the distance from the Schottky junction,[20,21]

$$\tilde{N}_T = 2\frac{\Delta C}{C_R}N_{d,net} = \frac{2}{w_R^2}\int_{x_{start}}^{x_{end}} xN_T(x)dx, \quad (1)$$

where ΔC and C_R are the DLTS or ICTS peak intensity of the electron trap and the steady-state capacitance, respectively. $N_{d,net}$ is the net donor density, and w_R is the depletion layer width when a measurement bias voltage (U_R) is applied for the Schottky junction. x_{start} denotes the start depth of the detection region, which is determined from the condition of the filling pulse in capacitance transient spectroscopy. x_{end} denotes the end depth of the detection region, which is determined from U_R in capacitance transient spectroscopy. Details regarding Eq. (1) are described in the Appendix.

In this study, the capacitance transient Fourier spectroscopy technique was employed,[22] and the b_1 coefficient was used as ΔC. In the region of $0\,\text{nm} < x \le x_{start}$ (no-electron-capture region), the electron traps do not capture electrons during the filling pulse period and the electron traps that exist in this region cannot be detected during the measurement period. Therefore, the electron traps in $x_{start} < x \le x_{end}$ can be detected and $\tilde{N}_T$ represents the averaged trap density in $x_{start} < x \le x_{end}$. When the lambda effect[12,15,21,23,24] during the filling pulse period and the measurement period is considered, i.e., the trap energy level in the depletion layer of $x_{start} < x \le w_P$ or $x_{end} < x \le w_R$ is below the Fermi level in the neutral region, x_{start} is given as $x_{start} = w_P - \lambda$ for $w_P > \lambda$ and $x_{start} = 0\,\text{nm}$ for $w_P \le \lambda$. x_{end} is given as $x_{end} = w_R - \lambda$. Here, w_P is the depletion layer width when the filing pulse bias voltage (U_P) is applied to the Schottky junction. In a basic case of constant electron trap density in the depth direction, the impact of the lambda effect on $\tilde{N}_T$ is discussed in the Appendix.

Assuming that the depth profile of an electron trap density generated during an RIE process has a distribution that decays exponentially from the etched surface in the depth direction,[25] $N_T(x)$ can be described as an equation based on

$$N_T(x) = N_T(0)\exp\left(-\frac{x}{L}\right). \quad (2)$$

Here, L is defined as the depth of carrier trap generation and $N_T(0)$ is the carrier trap density at the etched surface. The depth profile of an electron trap density is shown as a black solid line in Fig. 1(a). The dependence of the averaged trap density on the depletion layer width calculated from Eqs. (1) and (2) is also shown as a black broken line in Fig. 1(a). Figures 1(b) and 1(c) show band diagrams of an SBD with an assumed depth profile of trap density during the filling pulse period (upper side) and the measurement period (lower side) with U_R of U_{R1} and U_{R2} ($U_P > U_{R1} > U_{R2}$), respectively. The depletion layer widths during the measurement period with U_{R1} and U_{R2} are set to w_{R1} and w_{R2}, respectively. For simplicity, x_{start} is set to $w_P - \lambda$ in Fig. 1.

In the case of a carrier trap generated during an RIE process, not only the lambda effect but also the steep depth profile localized near the etched surface should be considered with respect to the dependence of the averaged trap density on the depletion layer width. When $x_{end} - x_{start} = (w_R - \lambda) - (w_P - \lambda)$, which is the width of the detection region, is smaller than or approximately the same length as λ [e.g., $w_R = w_{R1}$ in Fig. 1(b)], $\tilde{N}_T(w_R)$ is strongly affected by the lambda effect. The electron traps in the depletion layer during the measurement period are then localized near the etched surface. Therefore, $\tilde{N}_T(w_R)$ is also strongly affected by the steep depth profile of electron trap density. When $(w_R - \lambda) - (w_P - \lambda)$ is much larger than λ [e.g., $w_R = w_{R2}$ in Fig. 1(c)], the lambda effect on $\tilde{N}_T(w_R)$ becomes small because the number of electron trap in the no-electron-emission region, which is far from the etched surface as shown in Fig. 1(c), is negligible with respect to that in the detection region. As a consequence of $N_T(x)$, the averaged trap density $\tilde{N}_T(w_R)$ then decreases with increasing w_R.

$\tilde{N}_T(w_R)$ is determined in the competition between the lambda effect and the depth profile of the electron tarp density. Figure 1(a) shows that in this case with surface-localized $N_T(x)$, $\tilde{N}_T(w_R)$ has a maximum value at $w_R = 1.8\,\mu\text{m}$. It is crucial to appropriately determine the conditions for the filling pulse and the measurement pulse by considering the shape of the depth profile, the properties of the electron traps to be evaluated, and the structure of the SBD, such as the doping concentration of the epilayer and the Schottky barrier height.

III. EXPERIMENTS

N-doped, n-type 4H-SiC (0001) epilayers were used as starting materials for defect characterization. Inductively coupled plasma (ICP)-RIE was performed for 5 min under a typical condition [SF_6: 10 SCCM; O_2: 20 SCCM; Ar: 100 SCCM; ICP power: 900 W; bias power: 100 W; pressure: 2 Pa; etching rate: 0.6 μm/min], which resulted in the removal of a 3.0 μm thick layer. After the RIE process, all samples were cleaned in the RCA cleaning process.[26] To detect carrier traps generated during the RIE process with capacitance transient spectroscopy technique, Ni was deposited on the etched surfaces as Schottky contacts by using vacuum evaporation. The diameters of the Schottky electrodes were 1.5 mm. Aluminum was employed for backside ohmic contacts. $N_{d,net}$ of $1 \times 10^{15}\,\text{cm}^{-3}$ was determined from capacitance–voltage (C–V) measurements of the SBD using the epilayer.

For the RIE-etched sample, ICTS measurement was performed at 300 K to investigate electron traps. In the ICTS measurement, typical filling pulse bias voltage U_P and filling pulse width (t_P) were 1.5 V and 200 ms, respectively. The ICTS measurement was performed with various measurement bias voltages from 0 to −50 V. The detection limit of $\tilde{N}_T$ in the samples was $2 \times 10^{11}\,\text{cm}^{-3}$ using $\Delta C/C_R = 10^{-4}$.[27] To determine the energy positions of electron traps ($\Delta E_T = E_C - E_T$), DLTS measurements were performed in the temperature (T) range from 200 to 380 K with $U_P = 1.5\,\text{V}$

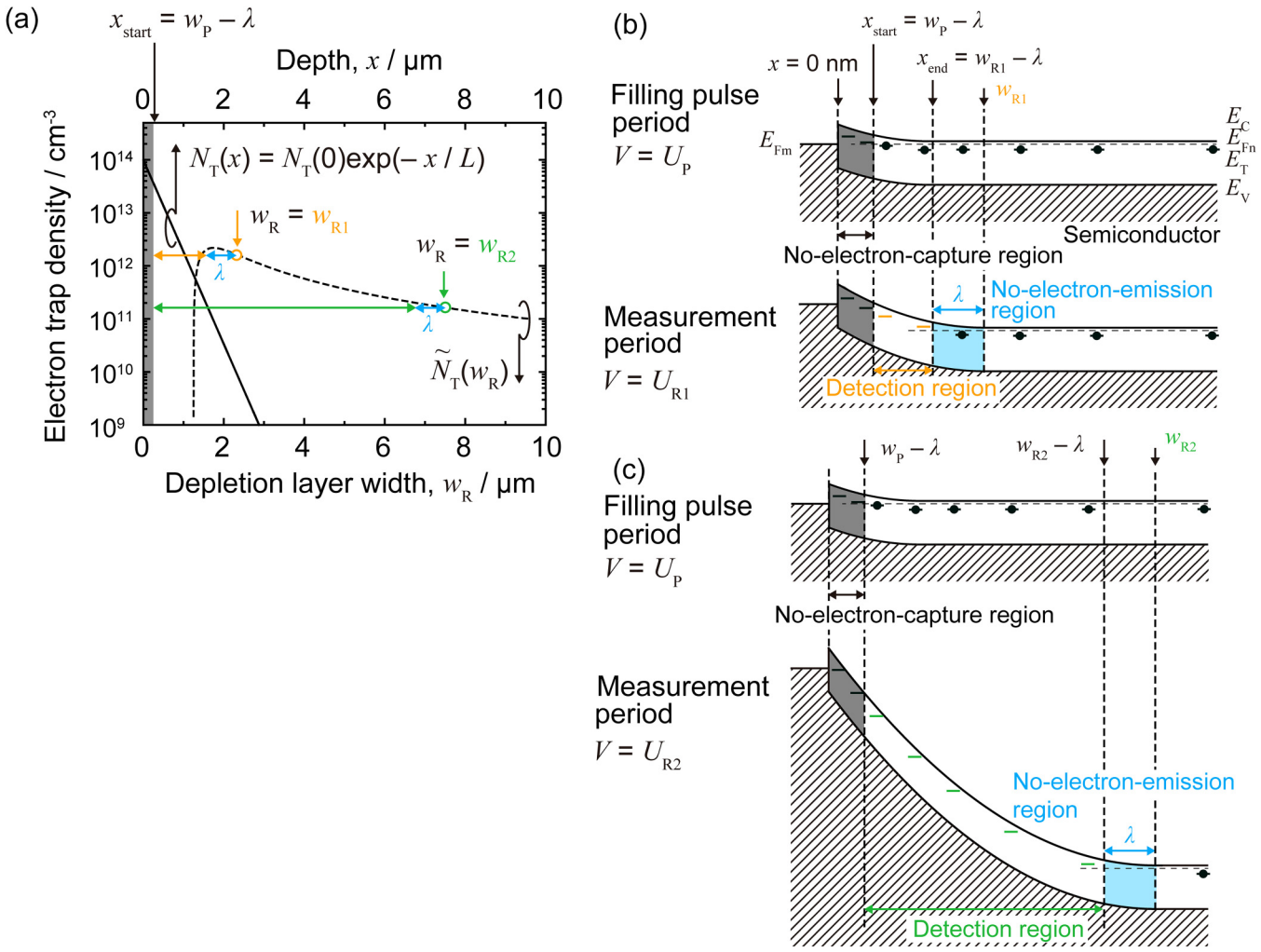

FIG. 1. Representative example for the approach of the proposed method. (a) Exponential depth profile of an electron trap density [$N_T(x) = N_T(0)\exp(-x/L)$; black solid line] and the dependence of the averaged trap density on the depletion layer width calculated from Eq. (1) [$\tilde{N}_T(w_R)$; black broken line]. Band diagrams of an SBD during the filling pulse period (upper side) and the measurement period (lower side) with measurement bias voltages of (b) U_{R1} and (c) U_{R2} ($U_{R1} > U_{R2}$).

and $t_P = 200$ ms. The measurement period widths were set to 20.5 ms, 205 ms, and 2.05 s, and a measurement bias voltage of −5 V was used in the DLTS measurement. To investigate electron traps that exist before the RIE process, ICTS and DLTS measurements were also performed for a Ni/n-type SiC SBD using the as-grown sample. Considering low electric field strength at the Schottky interface (<1 MV/cm), interface states do not affect DLTS and ICTS measurements in this study.

In the measurement principle, depth profiles can be extracted from either the DLTS or ICTS measurement with the proposed method. Here, the ICTS technique was selected because of the following two perspectives. From an experimental point of view, measurement with various bias voltages is required with this method. Therefore, it is difficult to apply the DLTS technique for this method. From an analytical point of view, to eliminate the impact of lambda effect dependence on temperature[12,15,21,23,24] and steady-state capacitance C_R from the obtained trap density, the ICTS technique is more suitable for this method. In this study, constant-voltage ICTS mode was used. On the other hand, when the measured carrier trap density $\tilde{N}_T$ is as high as the net donor density $N_{d,net}$, the constant-capacitance ICTS mode is useful to extract depth profiles of carrier trap density with the proposed method.

IV. RESULTS AND DISCUSSION

A. Electron traps detected in RIE-etched samples

Figure 2 shows ICTS spectra of (a) the as-grown sample and (b) the RIE-etched sample. In the as-grown sample, the $Z_{1/2}$ center

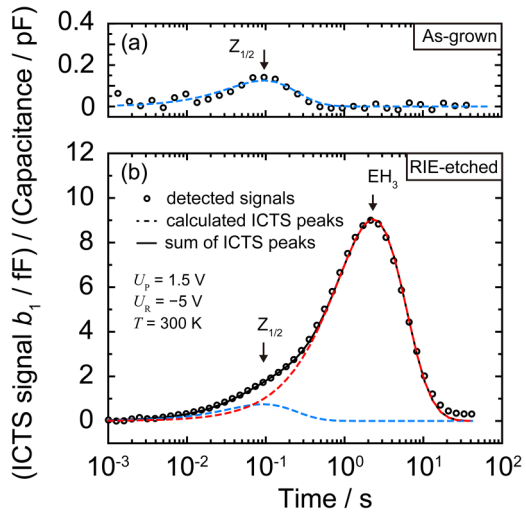

FIG. 2. ICTS spectra obtained at 300 K from (a) as-grown n-type 4H-SiC and (b) RIE-etched n-type 4H-SiC. The experimental ICTS spectra are indicated with open circles. The blue and red broken lines show calculated ICTS peaks for $Z_{1/2}$ and EH_3 centers, respectively. The black solid line shows the sum of the calculated ICTS peaks.

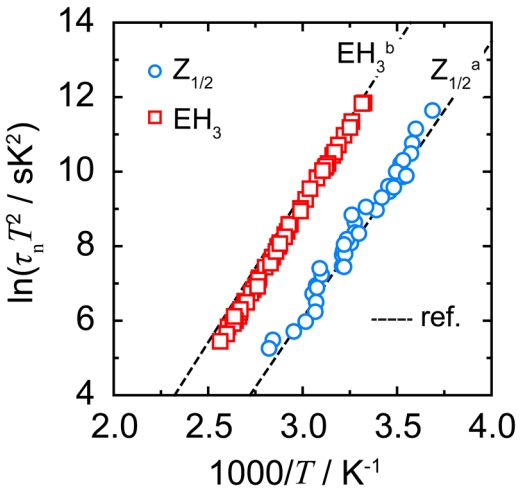

FIG. 3. Arrhenius plots of $\ln(\tau_n T^2)$ vs reciprocal temperature obtained from DLTS measurements for the $Z_{1/2}$ center (blue circles) and the EH_3 center (red squares). Reported Arrhenius plots of $\ln(\tau_n T^2)$ vs the reciprocal temperature for each electron trap are also shown as black broken lines. a represents Ref. 29 and b represents Ref. 31.

$(E_C - 0.64\,\text{eV})$[7,28,29] was detected and the $Z_{1/2}$ center density of $4.3 \times 10^{11}\,\text{cm}^{-3}$ was obtained from the ICTS data with the consideration of the lambda effect. After the RIE process, the EH_3 center $(E_C - 0.74\,\text{eV})$[17,30–32] emerged while the $Z_{1/2}$ center was also observed. Figure 3 shows the Arrhenius plots of $\ln(\tau_n T^2)$ vs the reciprocal temperature with the assumption that the electron capture cross section (σ_n) is independent of temperature, where τ_n is the time constant for electron emission from an electron trap to the conduction band. The energy positions and electron capture cross sections of the electron traps are summarized in Table I. The $Z_{1/2}$ center, which originates from carbon vacancies (V_C), has been observed in as-grown 4H-SiC layers.[18,28,29,33,35] The EH_3 center has been reported to be generated by electron or proton irradiation,[17,30–32,34] ion implantation,[9] or the RIE process.[19] The origin of the EH_3 center is considered to be carbon interstitial (C_i)-related defects because the EH_3 center was generated after irradiation with a low-energy electron (116 keV),[17,32] by which only carbon atoms may be displaced.[36] The analysis based on the diffusion-limited theory for the annealing behavior of EH_3 center also suggested that the EH_3 center is C_i-related.[32] In this study, we focused on these two contrasting electron traps.

B. Condition of filling pulse bias voltage

To investigate the depth profiles of electron traps generated during the RIE process, x_{start} in Eq. (1), which is the start depth of the detection region as shown in Fig. 1, must be sufficiently small because the etching damage should be localized near the etched surface. ICTS measurement was thus performed at 300 K and at $U_R = -5\,\text{V}$ with various filling pulse bias voltages to select an appropriate filling pulse condition.

Figure 4(a) shows the dependence of $w_P - \lambda$ on the filling pulse bias voltage for the $Z_{1/2}$ (blue circles) and EH_3 (red squares) centers in the RIE-etched sample. An electron trap with small ΔE_T shows a tendency to have a small lambda length due to its high thermal emission rate of electrons from the electron traps to the conduction band at a certain temperature. The filling pulse bias voltage that satisfies the condition of $w_P - \lambda = 0$ is higher in the case of the $Z_{1/2}$ center than the EH_3 center, which is consistent with λ of the $Z_{1/2}$ center being shorter, e.g., λ is 6.7×10^2 nm for the $Z_{1/2}$ center and 7.5×10^2 nm for the EH_3 center with $U_P = 0\,\text{V}$. Figure 4(b) shows the dependence of $\tilde{N}_T$ on the filling pulse bias voltage. The vertical axis in Fig. 4(b) is normalized with respect to $\tilde{N}_T$ obtained with $U_P = 2\,\text{V}$. The start depth of the detection region x_{start} decreases with increasing filling pulse bias voltage. Therefore, the detection region width $[x_{end} - x_{start} = (w_R - \lambda) - x_{start}]$ increases with increasing filling pulse bias voltage. $\tilde{N}_T$ also increases because the electron traps localized near the etched surface, which have a high density, become detectable. It should be noted that the dependence of the normalized $\tilde{N}_T$ on the filling pulse bias voltage reflects the actual depth profiles of each electron trap density. In Fig. 4(b), the normalized $\tilde{N}_T$ becomes saturated at unity when the filling pulse bias

TABLE I. Energy positions and electron capture cross sections of defect centers observed in RIE-etched n-type 4H-SiC.

Defect center	$E_C - E_T$ (eV)	σ_n (cm^2)
$Z_{1/2}$	0.64	4×10^{-15}
EH_3	0.74	8×10^{-15}

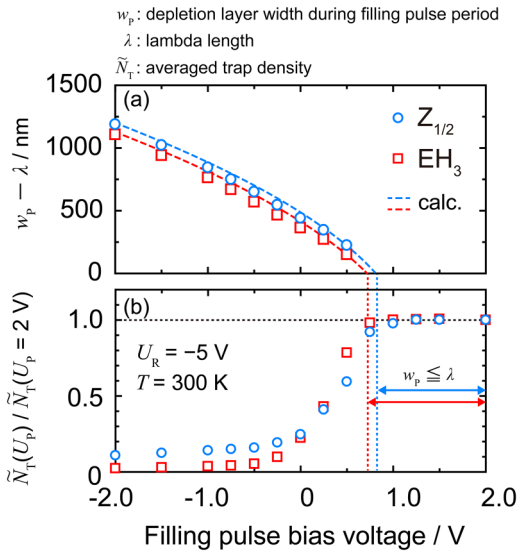

FIG. 4. (a) Difference between the depletion layer width and the lambda length ($w_P - \lambda$) for each defect center in the RIE-etched sample during the filling pulse period. The blue circles and the red squares indicate the $Z_{1/2}$ and EH_3 centers, respectively. The broken lines show the calculated dependence of ($w_P - \lambda$) on the filling pulse bias voltage for each electron trap using a Schottky barrier height of 1.5 eV. (b) Filling pulse bias voltage dependence of the averaged trap density obtained from the ICTS peak at a measurement bias voltage of −5 V. The blue circles and red squares indicate the $Z_{1/2}$ and EH_3 centers, respectively. The vertical axis is normalized with respect to the averaged trap density when the filling pulse bias voltage is 2 V. The color dotted lines denote the filling pulse bias voltage with $w_P - \lambda$ of 0 nm for each electron trap.

voltage is higher than the filling pulse bias voltage that satisfies the condition of $w_P - \lambda = 0$ nm. This result suggests that the trap energy level becomes lower than the quasi-Fermi level within the entire depletion layer during the filling pulse period. Therefore, electrons can be captured by the electron traps even near the Schottky interface during the filling pulse period.

On the other hand, an electron trap with an energy level located above the quasi-Fermi level in the depletion layer can be observed during the measurement period.[37] The barrier height of the SBD on the RIE-etched sample obtained from the C–V measurement is 1.5 eV, which is larger than the trap energy depth for electron traps detected in this study, and these trap energy levels are located above the quasi-Fermi level, except for the no-electron-emission region during the measurement period. The analysis was performed assuming that x_{start} is 0 nm when a filling pulse bias voltage of 1.5 V was employed, and each electron trap in $0\,\text{nm} < x \leq w_R - \lambda$ emits one electron during the measurement period.

C. Depth profiles of electron traps

It is preferable to satisfy the condition of $x_{start} = 0$ nm for obtaining the depth profile of the electron trap density near the etched surface. On the other hand, an increase in $x_{start} = w_P - \lambda$ allows only the depth profile of the electron trap density in the deeper region to be extracted. Extraction of a common depth profile of the electron trap density from the dependency of several averaged trap densities in the depletion layer width with various x_{start} can yield a depth profile with both a high-density distribution near the etched surface and a low-density distribution in the deeper region.

Figure 5 (red open squares) shows the dependence of the averaged EH_3 center density on depletion layer width in the RIE-etched sample obtained from the ICTS measurement at 300 K with (a) $U_P = 1.5$ V, (b) $U_P = 0$ V, and (c) $U_P = -4$ V with various U_R from 0 to −50 V. Schematic cross sections of the SBD during the filling pulse period (upper side) and the measurement period (lower side) with filling pulse voltages of (d) 1.5, (e) 0, and (f) −4 V are also shown. When $U_P = 1.5$ V is applied for the Schottky junction [Fig. 5(a)], the EH_3 center in $0\,\text{nm} < x \leq w_R - \lambda$ is detected in the ICTS measurement. For $U_P = 0$ V [Fig. 5(b)] and −4 V [Fig. 5(c)], $x_{start} = w_P - \lambda$ for the EH_3 center is 3.6×10^2 nm and 1.6 μm, respectively. When $\tilde{N}_T$ is compared at the same w_R, the averaged EH_3 center density decreases with decreasing filling pulse bias voltage because (1) the ratio of the detection region to the lambda length becomes small [Figs. 5(d)–5(f)] and the impact of the lambda effect becomes large and (2) the EH_3 center is localized near the etched surface.

The detected EH_3 center in Fig. 5(c) is located in the deeper region ($x > 1.6\,\mu$m). The depth profile of the EH_3 center density in the deeper region cannot be described from the depth profile of the single exponential in Eq. (2), which corresponds to that near the etched surface. In this study, the depth profile of the EH_3 center density is assumed to be a double exponential with a small generation depth L_1 and a large generation depth L_2,

$$N_T(x) = N_{T1}(0)\exp\left(-\frac{x}{L_1}\right) + N_{T2}(0)\exp\left(-\frac{x}{L_2}\right). \quad (3)$$

The exponential term with L_1 corresponds to the depth profile of the EH_3 center density near the etched surface, which indicates a non-channeling component. The exponential term with L_2 corresponds to the depth profile of the EH_3 center density in the deeper region, which indicates a channeling component. It is noted that the depth profiles can be reproduced to some extent by assuming the dual Pearson distribution function,[38] which is often used in the case of ion implantation (not shown). However, the dual Pearson distribution function needs much more parameters. Thus, the authors considered that the present double exponential function is a reasonable approximation.

The common depth profile of the EH_3 center density was extracted from the three different dependencies of the averaged EH_3 center density on the depletion layer width with different x_{start} shown in Figs. 5(a)–5(c), where x_{start} is 0 nm, 3.6×10^2 nm, and 1.6 μm, respectively. In the ICTS measurement, the maximum value of x_{end} is 7.0 μm for the EH_3 center when $U_R = -50$ V. Each $\tilde{N}_T(w_R)$ was calculated using the common $N_T(x)$ in Eq. (3), i.e., the parameters $N_{T1}(0)$, $N_{T2}(0)$, L_1, and L_2 are the same each other in Figs. 5(a)–5(c). Curve fitting with the calculated $\tilde{N}_T(w_R)$ [black broken lines in Figs. 5(a)–5(c)] to the measured $\tilde{N}_T(w_R)$

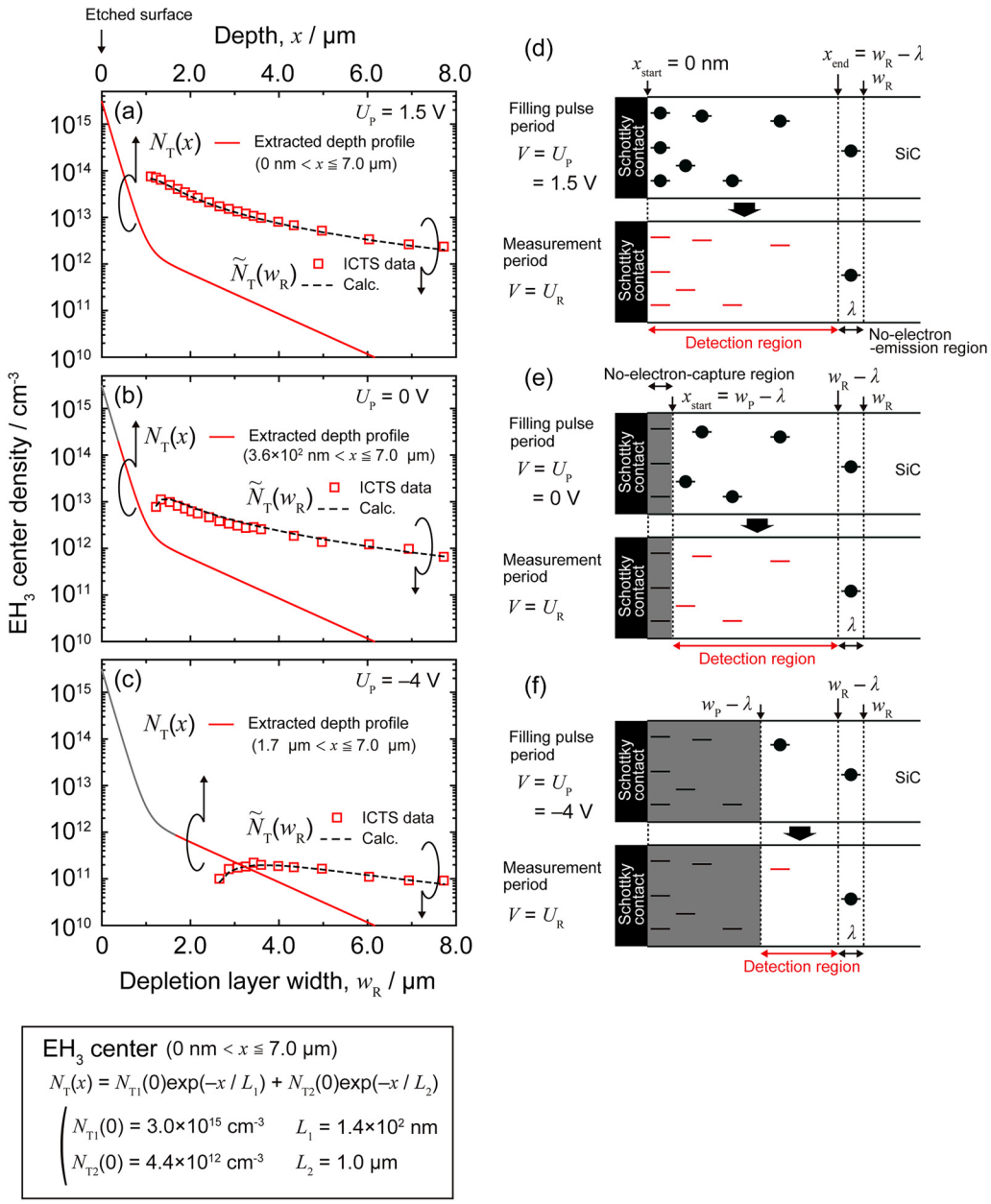

FIG. 5. Dependence of the averaged trap density obtained from ICTS measurements at 300 K for the EH_3 center in the RIE-etched sample on the depletion layer width with filling pulse voltages of (a) 1.5, (b) 0, and (c) −4 V. The open squares denote averaged EH_3 center densities calculated from the ICTS peaks. The black broken lines are fitting curves based on Eq. (3). The extracted depth profiles are shown as red solid lines. In (b) and (c), the depth profiles in undetectable regions are shown by gray solid lines. Schematic cross sections of an SBD during the filling pulse period (upper side) and the measurement period (lower side) with filling pulse bias voltages of (d) 1.5, (e) 0, and (f) −4 V.

[red squares in Figs. 5(a)–5(c)] was performed with the common fitting parameters, which are $N_{T1}(0)$, L_1, $N_{T2}(0)$, and L_2 in Eq. (3). The fitting parameters for the calculation are shown in Fig. 5. The extracted depth profile of the EH_3 center density is plotted in Figs. 5(a)–5(c) as red solid lines. When $U_P = 0$ V and $U_P = -4$ V are, respectively, applied, the EH_3 center for $0\,\text{nm} < x \leq 3.6 \times 10^2\,\text{nm}$ and $0\,\text{nm} < x \leq 1.6\,\mu\text{m}$ cannot be detected. The extracted depth profile of the EH_3 center density in the

no-electron-capture region is shown as gray solid lines in Figs. 5(b) and 5(c). Although the EH_3 center generated during the RIE process is localized near the etched surface ($x < 1\,\mu$m), the EH_3 center also exists in the deeper region ($x > 2\,\mu$m), where the density is low [$N_T(x) < 10^{12}\,cm^{-3}$]. The existence of the EH_3 center in the deeper region is confirmed to be valid from the ICTS measurement at $U_P = -4$ V [Fig. 5(c)], in which the EH_3 center is not detected near the etched surface ($0\,nm < x \leq 1.6\,\mu$m). The EH_3 center may be carbon-interstitial (C_i) atoms.[17,32] It is considered that the EH_3 centers generated during the RIE process originate from carbon atoms ejected from the etched region and accumulated in the SiC epilayer.

Figure 6 (blue open circles) shows the dependence of the averaged $Z_{1/2}$ center density on the depletion layer width in the RIE-etched sample obtained from the ICTS measurement at 300 K with (a) $U_P = 1.5$ V, (b) $U_P = 0$ V, and (c) $U_P = -4$ V. In the same way as that for the EH_3 center in Fig. 5, the depth profile of the $Z_{1/2}$ center density in the RIE-etched sample was extracted and is shown as blue solid lines in Fig. 6. x_{start} in Eq. (1) for the $Z_{1/2}$ center is 0 nm, 4.4×10^2 nm, and 1.7 μm with U_P of 1.5 [Fig. 6(a)], 0 [Fig. 6(b)], and −4 V [Fig. 6(c)], respectively. The maximum value of x_{end} is 7.1 μm for the $Z_{1/2}$ center when U_R of −50 V was used in the ICTS measurement. As the depth profile of $Z_{1/2}$ center density, a double exponential with a constant term is assumed:

$$N_T(x) = N_{T1}(0)\exp\left(-\frac{x}{L_1}\right) - N_{T2}(0)\exp\left(-\frac{x}{L_2}\right) + N_{T,as-grown}. \quad (4)$$

The two exponential terms and the constant term correspond to the $Z_{1/2}$ center generated during the RIE process and that existing before the RIE process, respectively, the fitting parameters of which are shown in Fig. 6. In the RIE-etched sample, a constant term $N_{T,as-grown}$ of $5.6 \times 10^{11}\,cm^{-3}$ is obtained and is almost identical to the $Z_{1/2}$ center density in the as-grown sample of $4.3 \times 10^{11}\,cm^{-3}$.

D. Discussion

The extracted depth profiles of the $Z_{1/2}$ center density (blue solid line) and the EH_3 center density (red solid line) are shown in Fig. 7. The blue and black broken lines denote the second exponential term, which has a larger generation depth L_2, and $N_{T,as-grown}$ in the depth profile of the $Z_{1/2}$ center density, respectively. Near the etched surface ($x < 800$ nm), the first exponential term, which has a smaller generation depth L_1, is dominant in the depth profiles of both the $Z_{1/2}$ center density and the EH_3 center density. L_1 of the $Z_{1/2}$ center (1.4×10^2 nm) is almost identical to that of the EH_3 center (1.4×10^2 nm), which suggests that the $Z_{1/2}$ center (V_C) is generated near the surface by high-energy ion bombardment during the RIE process, and the EH_3 center (C_i) is generated by carbon atoms ejected to the deeper region by ion bombardment. In the deeper region ($x \approx 1\,\mu$m), the $Z_{1/2}$ center density is lower than $N_{T,as-grown}$. On the other hand, consideration of the EH_3 center in the deeper region ($x > 1\,\mu$m) reveals that the second exponential term, which has a larger generation depth L_2, becomes dominant in the depth profile of the EH_3 center density. L_2 of the EH_3 center (1.0 μm)

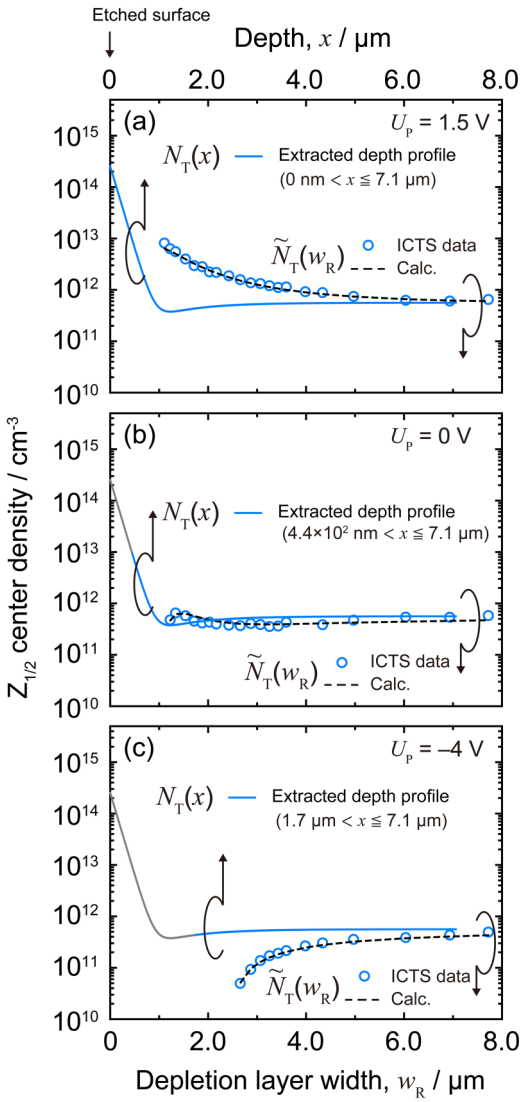

FIG. 6. Dependence of the averaged trap density obtained from ICTS measurements at 300 K for the $Z_{1/2}$ center in the RIE-etched sample on the depletion layer width with filling pulse voltages of (a) 1.5, (b) 0, and (c) −4 V. The open circles denote the averaged $Z_{1/2}$ center densities calculated from the ICTS peaks. The black broken lines are the fitting curves based on Eq. (4). The extracted depth profiles are shown as blue solid lines. In (b) and (c), the depth profiles in undetectable regions are shown by gray solid lines.

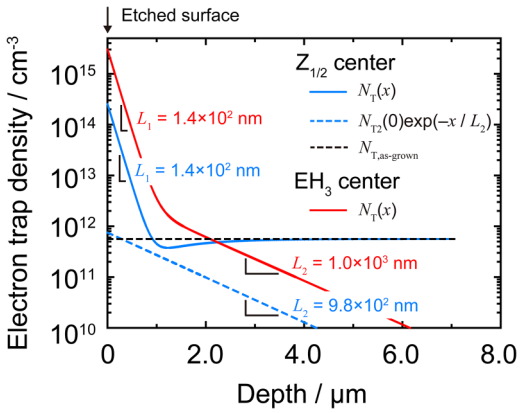

FIG. 7. Extracted depth profiles of the $Z_{1/2}$ center density (blue solid line) and the EH_3 center density (red solid line). The blue and black broken lines are the second exponential term and the constant term of the depth profile of the $Z_{1/2}$ center density, respectively.

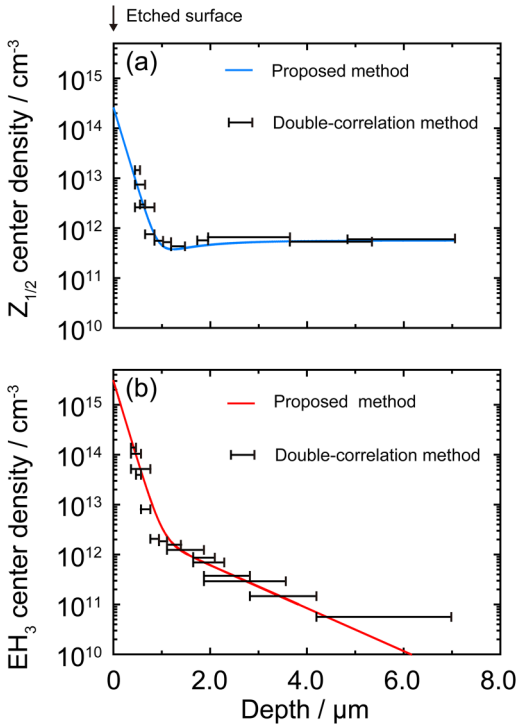

FIG. 8. Depth profiles of (a) the $Z_{1/2}$ center and (b) the EH_3 center. The color solid lines show the depth profiles extracted from the dependence of the averaged defect density on the depletion layer width. The black solid lines are depth profiles obtained with the double-correlation method.

is very similar to that of the $Z_{1/2}$ center (9.8×10^2 nm). This result suggests that in the deeper region ($x > 1\,\mu$m), (1) few V_C defects (the $Z_{1/2}$ center) are generated by ion bombardment during the RIE process, and (2) pair annihilation of V_C defects, which are present before the RIE process, and ejected carbon atoms, of which the depth profile is similar to that of the EH_3 center (C_i) density, occurs.

The depth profiles of (a) the $Z_{1/2}$ and (b) EH_3 center densities extracted by the proposed method (color solid lines) and obtained using the double-correlation method (black solid lines)[14,16] are shown in Fig. 8. In the double-correlation method, a depth profile of the electron trap density can be obtained without assuming a shape of the depth profile using the following steps: (1) the detection region ($w_P - \lambda < x \leq w_R - \lambda$) is adjusted to be small using an appropriate filling pulse bias voltage and an appropriate measurement bias voltage; (2) it is assumed that the trap density in the small detection region is constant; and (3) the averaged trap density obtained from the ICTS peak is corrected with respect to the lambda effect during both the filling pulse period and the measurement period. In the double-correlation method, when the depletion layer width is small and the detection region is close to the etched surface, where the depth profile shows a sharp drop, the difference in filling pulse bias voltages was chosen to be small so that a high spatial resolution is held. On the other hand, when the depletion layer width is large and the detection region is deeper, where the trap density is low, the difference in filling pulse bias voltages was chosen to be large so that a high-density resolution is achieved. Figure 8 shows that the depth profiles of the $Z_{1/2}$ and EH_3 center densities extracted from the dependence of $\tilde{N}_T$ on the depletion layer width are consistent with those determined by the double-correlation method in the density range larger than 10^{11} cm^{-3}. The double-correlation method has a trade-off relationship between the depth resolution and resolution in the trap density due to the measurement principle. However, with the proposed method, the trade-off relationship is relieved and a reasonable depth profile of trap density can be extracted by the measurement and the analysis of the dependence of $\tilde{N}_T$ on the depletion layer width when an appropriate function shape for the depth profile is assumed.

V. SUMMARY

In this study, the depth profiles of electron traps generated in n-type 4H-SiC during the RIE process were investigated. In the RIE-etched samples, two electron traps, the $Z_{1/2}$ and EH_3 centers, were detected in ICTS measurements at 300 K. Depth profiles of trap density can be extracted with the proposed method from the dependence of the averaged trap density on the depletion layer width. When a function based on an exponential is assumed as the depth profile, electron trap densities near the etched surface of 10^{14} to 10^{15} cm^{-3} and the depth of electron trap generation at 1.4×10^2 nm were obtained with the proposed method using the ICTS technique for the RIE-etched sample. The electron traps generated during the RIE process were confirmed to be localized near the etched surface ($x \leq 1\,\mu$m). A comparison of the extracted depth profile of the $Z_{1/2}$ center density to that of the EH_3 center density in the deeper region ($x > 1\,\mu$m) suggested that the pair annihilation of carbon vacancy defects and carbon atoms ejected by ion bombardment during the RIE process occurs. The proposed method is useful to

investigate the depth profile of carrier trap density when the carrier trap has a large depth direction distribution.

ACKNOWLEDGMENTS

This work was supported by "Program on Open Innovation Platform with Enterprises, Research Institute and Academia (OPERA)" of the Japan Science and Technology Agency (JST).

APPENDIX: AVERAGED CARRIER TRAP DENSITY IN DLTS AND IN ICTS

When an n-type SBD is used to investigate electron traps with DLTS or ICTS measurements, the electron trap density calculated from the DLTS or ICTS peak height ($\tilde{N}_T$) has the following relationship with the depth profile of actual trap density $N_T(x)$,[20,21]

$$\tilde{N}_T = 2\frac{\Delta C}{C_R}N_{d,net} = \frac{2}{w_R^2}\int_{x_{start}}^{x_{end}} xN_T(x)[f(x,0) - f(x,\infty)]dx. \quad (A1)$$

$f(x, t)$, where t is time from the application of the measurement bias voltage, is the time evolution of the depth profile of the electron occupancy ratio of the electron traps. The electron traps in $x_{start} < x \le x_{end}$ can be detected. In Eq. (A1), the following assumptions are typically made: (1) ΔC is small compared with C_R and (2) $N_{d,net}$ is a function that varies slowly in the range of $x_{start} < x \le x_{end}$. In this study, the following assumption is also made: (3) each electron trap in $x_{start} < x \le x_{end}$ emits one electron during the measurement period, which is sufficiently longer than the time constant of electron thermal emission from the electron trap to the conduction band (τ_n), i.e., $f(x, 0) = 1$ and $f(x, \infty) = 0$ in $x_{start} < x \le x_{end}$. $\tilde{N}_T$ obtained from Eq. (A1) is not equal to actual trap density N_T and is the averaged trap density in the entire depletion layer when the measurement bias voltage is applied. Considering that electrons in the conduction band are captured by electron traps in the depletion layer under the application of measurement bias voltage, $f(x, t)$ can be approximated as follows:[20,21]

$$\begin{aligned} f(x,t) &= f(x,0) - \left[f(x,0) - \frac{n(x,w)\sigma_n v_{th,n}}{e_n + n(x,w)\sigma_n v_{th,n}}\right]\left\{1 - \exp\left[-\frac{t}{1/(e_n + n(x,w)\sigma_n v_{th,n})}\right]\right\} \\ &\cong \begin{cases} \exp\left(-\dfrac{t}{1/e_n}\right), & x_{start} < x \le w - \lambda \\ 1, & w - \lambda < x \le w \end{cases}. \end{aligned} \quad (A2)$$

Here, $e_n = 1/\tau_n$ is the thermal emission rate of electrons from the electron traps to the conduction band, w is the depletion layer width, and $v_{th,n}$ is the electron thermal velocity. $n(x, w)$ is the free carrier concentration, assuming that[21,24]

$$n(x,w) = \begin{cases} N_{d,net}(w)\exp\left(-\dfrac{(w-x)^2}{2L_D(w)^2}\right), & 0 < x < w \\ N_{d,net}(x), & w \le x \end{cases}. \quad (A3)$$

Here, $L_D(w) = \sqrt{\varepsilon_s k_B T/n(w,w)e^2}$ is the Debye length and ε_s is the static permittivity and the static permittivity of 4H-SiC in the direction parallel to the c axis $\varepsilon_s^{\parallel} = 10.3\varepsilon_0$, where ε_0 is the vacuum permittivity. $\varepsilon_s^{\parallel}$ is obtained using the Lyddane–Sachs–Teller relation,[39] where the optical permittivity of 4H-SiC in the direction parallel to the c axis ($\varepsilon_\infty^{\parallel}$) is $6.78\varepsilon_0$,[40] and the optical-phonon angular frequencies of the A_{1T} mode and the A_{1L} mode ($\omega_{T,L}^{\parallel}$) are 783 and 964.2 cm^{-1}, respectively.[40] k_B is the Boltzmann constant. In Eq. (A3), it is assumed that the donor is completely ionized. In Eq. (A2), $w - \lambda$ is the depth where the trap energy level crosses the bulk Fermi level, i.e., the trap energy level in the depletion layer of $w - \lambda < x \le w$ is below the Fermi level in the neutral region, and $f(w - \lambda, \infty) = 0.5$. λ is given as[24]

$$\lambda(w) = L_D(w)\sqrt{2\ln\left(\frac{N_{d,net}(w)\sigma_n v_{th,n}}{e_n}\right)}. \quad (A4)$$

In $w_R - \lambda(w_R) < x \le w_R$, the electron traps emit very few electrons because the trap energy level is located below the quasi-Fermi level. This phenomenon is called the lambda effect.[12,15,21,23,24] It is noted that the magnitude of the lambda effect depends on e_n^t and σ_n of the electron trap and n, which is assumed to be equal to $N_{d,net}$ in this study. In this study, $\lambda(w_P)$ and $\lambda(w_R)$ are considered to be equal $[\lambda = \lambda(w_P) = \lambda(w_R)]$. Considering the lambda effect, Eq. (A1) can be approximated as

$$\tilde{N}_T = 2\frac{\Delta C}{C_R}N_{d,net} = \frac{2}{w_R^2}\int_{x_{start}}^{w_R - \lambda(w_R)} xN_T(x)dx. \quad (A5)$$

In $0 < x \le x_{start}$, the electron traps do not capture electrons during the filling pulse period and the electron traps cannot be detected during the measurement period. When the lambda effect

during the filling pulse period is considered, x_{start} is given as

$$x_{start} = \begin{cases} 0, & w_P \le \lambda(w_P) \\ w_P - \lambda(w_P), & \lambda(w_P) < w_P \end{cases}. \quad \text{(A6)}$$

When the depth profile of an electron trap density has a constant distribution, i.e., $N_T(x) = N_T$, the dependence of the averaged trap density on the depletion layer width $\tilde{N}_T(w_R)$ is influenced by the lambda effect. $\tilde{N}_T(w_R)$ calculated from Eq. (1) or Eq. (A5) using $N_T(x) = N_T$ is shown in Fig. 9(a). Here, the two depletion layer widths, the small depletion layer w_{R1} and the large depletion layer w_{R2}, are considered to explain the lambda effect on $\tilde{N}_T(w_R)$. Figures 9(b) and 9(c) show band diagrams of an SBD with an assumed depth profile of trap density during the filling pulse period (upper side) and the measurement period (lower side) with U_R of U_{R1} and U_{R2} ($U_P > U_{R1} > U_{R2}$), respectively. The depletion layer widths during the measurement period with U_{R1} and U_{R2} are set to w_{R1} and w_{R2}, respectively. For simplicity, x_{start} is set to $w_P - \lambda$ in Fig. 9. Figure 9(b) shows that when the depletion layer width is small, the width of the no-electron-capture region and the width of the no-electron-emission region, where the electron traps cannot be detected by capacitance transient spectroscopy, cannot be negligible with respect to the width of the detection region. Therefore, the averaged trap density $\tilde{N}_T$ is strongly underestimated compared to true trap density N_T. On the other hand, as shown in Fig. 9(c), when the depletion layer width is large, the width of the no-electron-capture region and the width of the

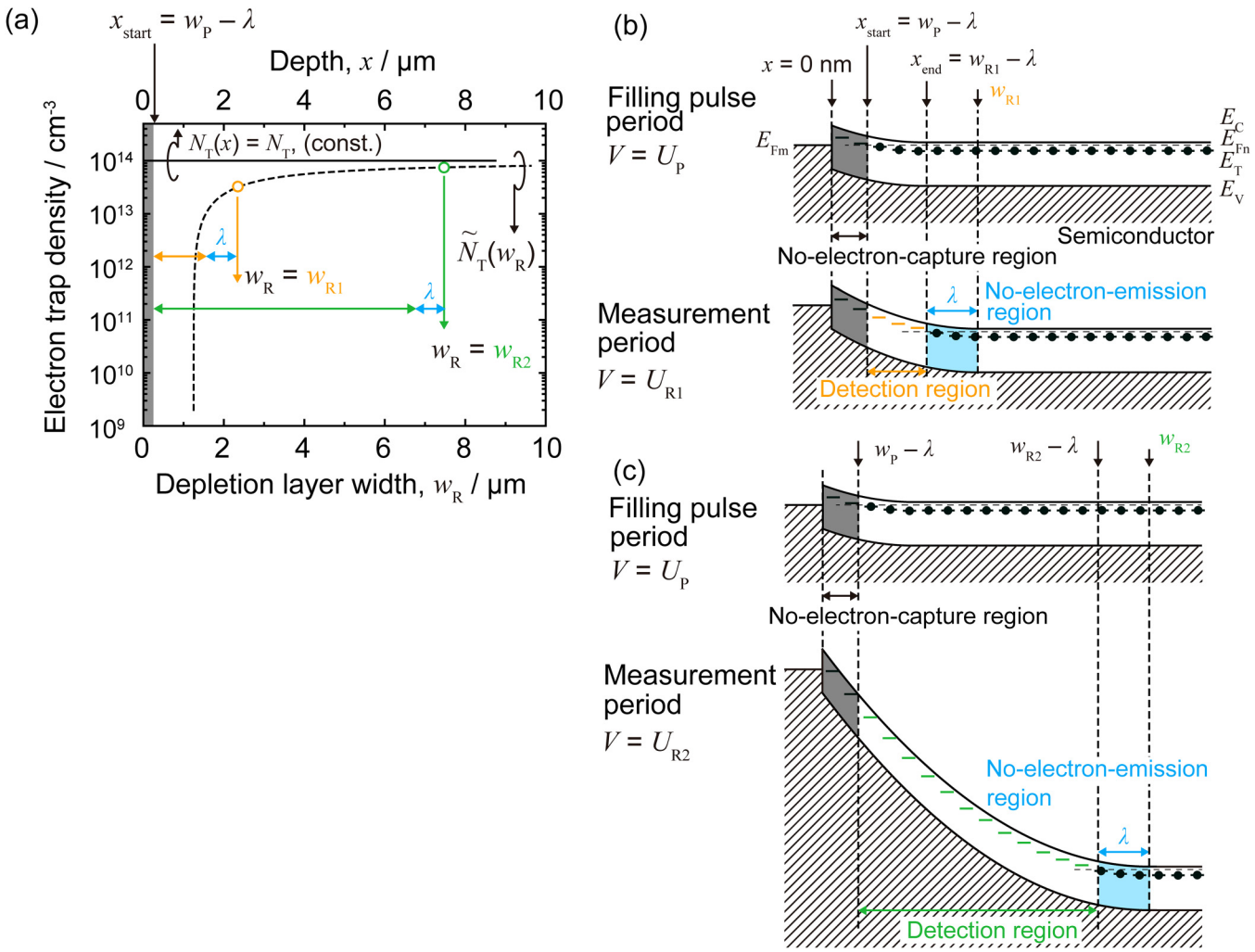

FIG. 9. Representative example for the lambda effect. (a) Constant depth profile of an electron trap density [$N_T(x) = N_T$; black solid line] and the dependence of the averaged trap density on the depletion layer width calculated from Eq. (1) [$\tilde{N}_T(w_R)$; black broken line]. Band diagrams of an SBD during the filling pulse period (upper side) and the measurement period (lower side) with measurement bias voltages of (b) U_{R1} and (c) U_{R2} ($U_{R1} > U_{R2}$).

no-electron-emission region can be negligible with respect to the width of the detection region. Therefore, the lambda effect can be negligible in the averaged trap density $\tilde{N}_T$. $\tilde{N}_T(w_R)$, where the trap density is constant in the depth direction, increases with increasing w_R, and $\tilde{N}_T(w_R)$ is asymptotic to N_T as shown in Fig. 9(a).

It is typically assumed that carrier traps are uniformly distributed in as-grown materials[12,13] or that the carrier trap density is constant in the detection region ($w_P - \lambda < x \leq w_R - \lambda$) in the case of carrier traps generated during device processes or electron irradiation.[9,16–19]

DATA AVAILABILITY

The data that support the findings of this study are available from the corresponding author upon reasonable request.

REFERENCES

[1]J. A. Cooper and A. Agarwal, Proc. IEEE **90**, 956 (2002).
[2]T. Kimoto, A. Itoh, N. Inoue, O. Takemura, T. Yamamoto, T. Nakajima, and H. Matsunami, Mater. Sci. Forum **264-268**, 675 (1998).
[3]B. J. Baliga, *Fundamentals of Power Semiconductor Devices* (Springer, New York, 2008).
[4]T. Kimoto and J. A. Cooper, *Fundamentals of Silicon Carbide Technology* (Wiley, Singapore, 2014).
[5]T. Kimoto, Jpn. J. Appl. Phys. **58**, 018002 (2019).
[6]V. Khemka, T. P. Chow, and R. J. Gutmann, J. Electron. Mater. **27**, 1128 (1998).
[7]T. Dalibor, G. Pensl, H. Matsunami, T. Kimoto, W. J. Choyke, A. Schöner, and N. Nordell, Phys. Status Solidi A **162**, 199 (1997).
[8]T. Troffer, M. Schadt, T. Frank, H. Itoh, G. Pensl, J. Heindl, H. P. Strunk, and M. Maier, Phys. Status Solidi A **162**, 277 (1997).
[9]K. Kawahara, G. Alfieri, and T. Kimoto, J. Appl. Phys. **106**, 013719 (2009).
[10]D. V. Lang, J. Appl. Phys. **45**, 3023 (1974).
[11]H. Okushi and Y. Tokumaru, Jpn. J. Appl. Phys. **20**, 261 (1981).
[12]R. R. Senechal and J. Basinski, J. Appl. Phys. **39**, 4581 (1968).
[13]K. Kanegae, M. Horita, T. Kimoto, and J. Suda, Appl. Phys. Express **11**, 071002 (2018).
[14]H. Lefèvre and M. Schulz, Appl. Phys. **12**, 45 (1977).
[15]Y. Zohta and M. O. Watanabe, J. Appl. Phys. **53**, 1809 (1982).
[16]A. Usami, Y. Tokuda, M. Katayama, S. Kaneshima, and T. Wada, J. Phys. D: Appl. Phys. **19**, 1079 (1986).
[17]K. Danno and T. Kimoto, J. Appl. Phys. **100**, 113728 (2006).
[18]L. Storasta, H. Tsuchida, T. Miyazawa, and T. Ohshima, J. Appl. Phys. **103**, 013705 (2008).
[19]K. Kawahara, M. Krieger, J. Suda, and T. Kimoto, J. Appl. Phys. **108**, 023706 (2010).
[20]D. Pons and S. Makram-Ebeid, J. de Phys. **40**, 1161 (1979).
[21]G. M. Martin, A. Mitonneau, D. Pons, A. Mircea, and D. W. Woodward, J. Phys. C: Solid State Phys. **13**, 3855 (1980).
[22]S. Weiss and R. Kassing, Solid-Sate Electron. **31**, 1733 (1988).
[23]C. T. Sah and V. G. K. Reddi, IEEE Trans. Electron Devices **11**, 345 (1964).
[24]S. D. Brotherton, Solid-State Electron. **26**, 987 (1983).
[25]S. Yamada, M. Omori, H. Sakurai, Y. Osada, R. Kamimura, T. Hashizume, J. Suda, and T. Kachi, Appl. Phys. Express **13**, 016505 (2020).
[26]W. Kern, J. Electrochem. Soc. **137**, 1887 (1990).
[27]P. Blood and J. W. Orton, *The Electrical Characterization of Semiconductors: Majority Carriers and Electron States* (Academic Press, 1992).
[28]T. Kimoto, A. Itoh, H. Matsunami, S. Sridhara, L. L. Clemen, R. P. Devaty, W. J. Choyke, T. Dalibor, C. Peppermüller, and G. Pensl, Appl. Phys. Lett. **67**, 2833 (1995).
[29]J. Zhang, L. Storasta, J. P. Bergman, N. T. Son, and E. Janzén, J. Appl. Phys. **93**, 4708 (2003).
[30]C. Hemmingsson, N. T. Son, O. Kordina, J. P. Bergman, E. Janzén, J. L. Lindström, S. Savage, and N. Nordell, J. Appl. Phys. **81**, 6155 (1997).
[31]G. Alfieri, E. V. Monakhov, B. G. Svensson, and A. Hallén, J. Appl. Phys. **98**, 113524 (2005).
[32]G. Alfieri and A. Mihaila, J. Phys.: Condens. Matter **32**, 465703 (2020).
[33]N. T. Son, X. T. Trinh, L. S. Løvlie, B. G. Svensson, K. Kawahara, J. Suda, T. Kimoto, T. Umeda, J. Isoya, T. Makino, T. Ohshima, and E. Janzén, Phys. Rev. Lett. **109**, 187603 (2012).
[34]L. Storasta, J. P. Bergman, E. Janzén, A. Henry, and J. Lu, J. Appl. Phys. **96**, 4909 (2004).
[35]K. Kawahara, X. T. Trinh, N. T. Son, E. Janzén, J. Suda, and T. Kimoto, Appl. Phys. Lett. **102**, 112106 (2013).
[36]H. J. von Bardeleben, J. L. Cantin, L. Henry, and M. F. Barthe, Phys. Rev. B **62**, 10841 (2000).
[37]S. A. Reshanov, G. Pensl, K. Danno, T. Kimoto, S. Hishiki, T. Ohshima, H. Itoh, F. Yan, R. P. Devaty, and W. J. Choyke, J. Appl. Phys. **102**, 113702 (2007).
[38]A. F. Tasch, H. Shin, C. Park, J. Alvis, and S. Novak, J. Electrochem. Soc. **136**, 810 (1989).
[39]R. H. Lyddane, R. G. Sachs, and E. Teller, Phys. Rev. **59**, 673 (1941).
[40]H. Harima, S. Nakashima, and T. Uemura, J. Appl. Phys. **78**, 1996 (1995).